

Hierarchy and size distribution function of star formation regions in the spiral galaxy NGC 628

Alexander S. Gusev

Sternberg Astronomical Institute, Lomonosov Moscow State University, Universitetsky pr. 13, 119992 Moscow, Russia, gusev@sai.msu.ru

Accepted 2014 June 2. Received 2014 June 2; in original form 2013 December 24

ABSTRACT

Hierarchical structures and size distribution of star formation regions in the nearby spiral galaxy NGC 628 are studied over a range of scale from 50 to 1000 pc using optical images obtained with 1.5 m telescope of the Maidanak Observatory. We found hierarchically structured concentrations of star formation regions in the galaxy, smaller regions with a higher surface brightness are located inside larger complexes having a lower surface brightness. We illustrate this hierarchy by dendrogram, or structure tree of the detected star formation regions, which demonstrates that most of these regions are combined into larger structures over several levels. We found three characteristic sizes of young star groups: ≈ 65 pc (OB associations), ≈ 240 pc (stellar aggregates) and ≈ 600 pc (star complexes). The cumulative size distribution function of star formation regions is found to be a power law with a slope of approximately -1.5 on scales appropriate to diameters of associations, aggregates and complexes. This slope is close to the slope which was found earlier by B. Elmegreen et al. for star formation regions in the galaxy on scales from 2 to 100 pc.

Key words: H II regions – galaxies: individual: NGC 628 (M74)

1 INTRODUCTION

As is known, such physical processes as gravitational collapse and turbulence compression play a key role in creation and evolution of star formation regions over the wide range of scales, from star complexes over OB associations down to compact embedded clusters and to clumps of young stars inside them. These stellar systems form a continuous hierarchy of structures for all these scales (Efremov 1995; Efremov & Elmegreen 1998; Elmegreen et al. 2000; Elmegreen 2002, 2006, 2011). It is suggested that the hierarchy extends up to 1 kpc (Efremov, Ivanov & Nikolov 1987; Elmegreen & Efremov 2006; Zhang, Fall & Whitmore 2001).

Efremov et al. (1987) and Ivanov (1991) described at least three categories of hierarchical star groups on the largest levels: OB associations with a length scale ≈ 80 pc, stellar aggregates with a length scale ≈ 250 pc and star complexes with diameters ≈ 600 pc. H I/H₂ superclouds are ancestors of star complexes; OB associations are formed from giant molecular clouds (Efremov 1989, 1995; Efremov & Elmegreen 1998; Elmegreen 1994; Elmegreen & Efremov 2006; Elmegreen 2009; Odekon 2008; de la Fuente Marcos & de la Fuente Marcos 2009). Sizes and clustering of these structures have been studied for many nearby spiral and irregular galaxies (Bastian et al. 2005; Bianchi et al. 2012; Battinelli 1991; Battinelli, Efremov & Magnier 1996; Borissova et al. 2004; Bresolin, Kennicutt & Stetson 1996; Bresolin et al. 1998; Bruevich, Gusev & Guslyakova 2011; Elmegreen & Elmegreen 2001; Feitzinger & Braunsfurth

1984; Gouliermis et al. 2010; Gusev 2002; Harris & Zaritsky 1999; Magnier et al. 1993; Pietrzyński et al. 2001, 2005; Sánchez et al. 2010; Wilson 1991, 1992). Power-law power spectra of optical light in galaxies suggest the same maximum scale, possibly including the ambient galactic Jeans length (Elmegreen, Elmegreen & Leitner 2003a; Elmegreen et al. 2003b). If the ambient Jeans length is the largest scale, then a combination of gravitational and turbulent fragmentations can drive the whole process. Observed star formation rates in galaxies can follow from such turbulent structures (Krumholz & McKee 2005).

Hierarchical clustering disappears with age as stars mix. The densest regions have the shortest mixing times and lose their substructures first. Nevertheless, very young clusters have a similar pattern of subclustering, suggesting that this structure continues down to individual stars (Brandeker, Jayawardhana & Najita 2003; Dahm & Simon 2005; Heydari-Malayeri et al. 2001; Kumar, Kamath & Davis 2004; Oey et al. 2005; Sánchez-Monge et al. 2013).

The interstellar matter also shows a hierarchical structure from the largest giant molecular clouds down to individual clumps and cores. The complex hierarchical structure of the interstellar matter is shaped by supersonic turbulence (Ballesteros-Paredes et al. 2007). The scaling relations observed in molecular clouds (Larson 1981) can be explained by the effect of turbulence, where energy is injected at largest scales and cascades down to the smallest scales, creating eddies and leading to a hierarchical structure on

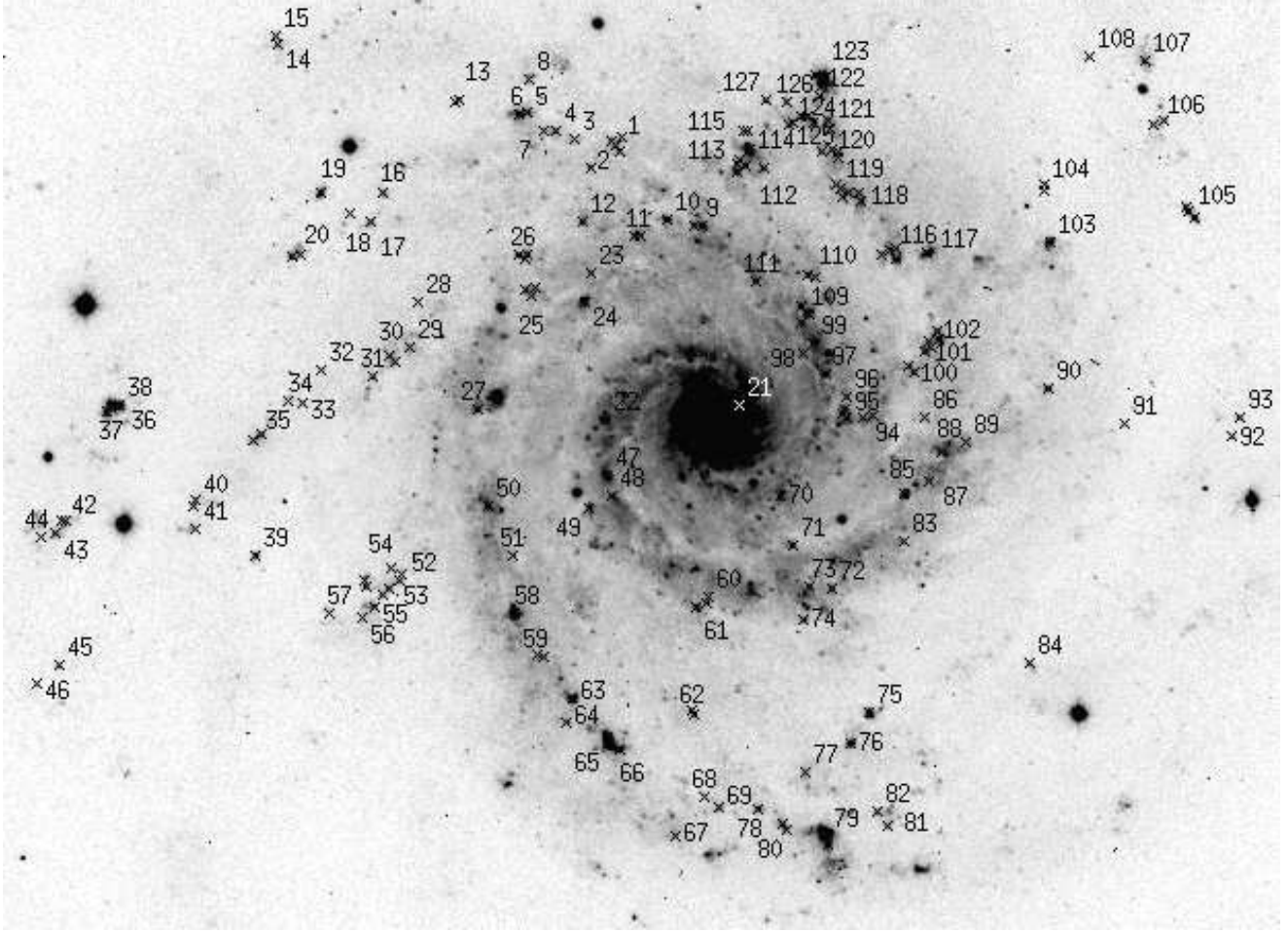


Figure 1. *B* image of NGC 628 and positions of the galaxy's star formation regions (crosses). The numbers of the star formation regions from Table A1 are indicated. The image size is 8.26×6.00 arcmin. North is upward and east is to the left.

Table 1. Basic parameters of NGC 628.

Parameter	Value
Type	Sc
RA (J2000.0)	$01^h 36^m 41.81^s$
DEC (J2000.0)	$+15^\circ 47' 00.3''$
Total apparent <i>B</i> magnitude (B_T)	9.70 mag
Absolute <i>B</i> magnitude (M_B) ^a	-20.72 mag
Inclination (<i>i</i>)	7°
Position angle (PA)	25°
Apparent corrected radius (R_{25}) ^b	5.23 arcmin
Apparent corrected radius (R_{25}) ^b	10.96 kpc
Distance (<i>D</i>)	7.2 Mpc

^a Absolute magnitude of a galaxy corrected for Galactic extinction and inclination effect.

^b Isophotal radius (25 mag arcsec⁻² in the *B*-band) corrected for Galactic extinction and absorption due to the inclination of NGC 628.

all scales (Elmegreen et al. 2006). It is believed that turbulence plays a major role in star formation; it creates density enhancements that become gravitationally unstable and collapse to form stars (Elmegreen et al. 2006). The spatial distribution of young

stars and stellar groups on wide length scales probably reflects this process.

The purpose of this paper is to study size distribution and hierarchical structures of star formation regions (SFRs) in nearby face-on spiral galaxy NGC 628 (Fig. 1), based on our own observations in the *U*, *B*, and *V* passbands. This galaxy is an excellent example of a galaxy with numerous star formation regions observed at different length scales. We use the term 'star formation regions', which includes young star complexes, OB associations, H II regions, i.e. all young stellar groups regardless of their sizes.

Hodge (1976) identified 730 H II regions in the galaxy. Ivanov et al. (1992) estimated sizes and magnitudes of 147 young stellar associations and aggregates in NGC 628 and discussed briefly hierarchical structures at the scales from 50 to 800 pc. Larsen (1999) studied 38 young star clusters with an effective diameters from 2 to 90 pc. Bruevich et al. (2007) obtained magnitudes, colours and sizes of 186 SFRs based on the list of H II regions from Belley & Roy (1992).

Elmegreen et al. (2006) studied distributions of size and luminosity of star formation regions over a range of scales from 2 to 110 pc using progressively blurred versions of blue optical and H α images from the *Hubble Space Telescope* (*HST*). They counted and measured features in each blurred image using SExtractor program and found that the cumulative size distribution satisfies a power

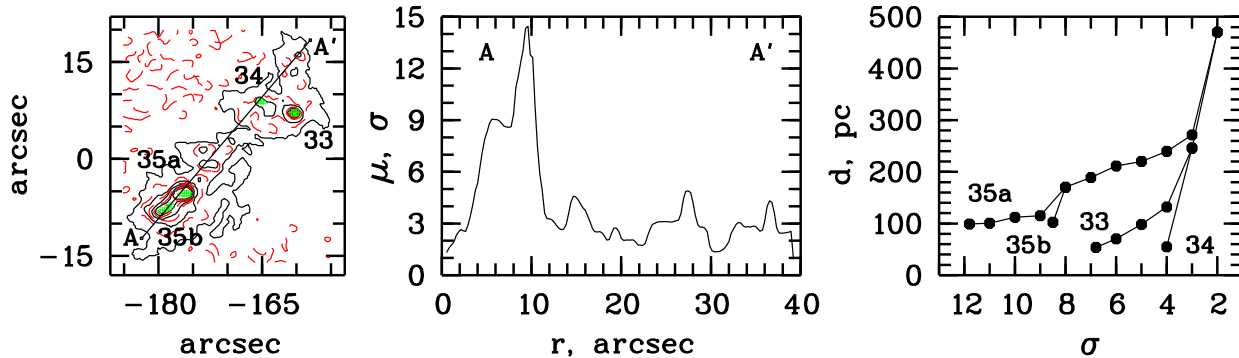


Figure 2. Left panel: contour map of the vicinity of SFRs Nos. 33-35. Grey areas correspond to the regions Nos. 33, 34, 35a, and 35b within their half-maximum brightness level. Red dashed contour levels correspond to the levels of σ , 3σ , 5σ , 7σ , and 9σ , black solid contour levels correspond to the levels of 2σ , 4σ , 6σ , 8σ , and 10σ above the average brightness level of background. Position of profile A–A' is shown. Central panel: photometric profile A–A'. Surface brightness, μ , is given in units of σ . Right panel: diameters of SFRs Nos. 33-35 and their hierarchical structures measured at the different levels of surface brightness in units of σ .

law with a slope of approximately from -1.8 to -1.5 on all studied scales.

The fundamental parameters of NGC 628 are presented in Table 1. We take the distance to NGC 628, obtained in Sharina, Karachentsev & Tikhonov (1996) and van Dyk, Li & Filippenko (2006). We used the position angle and the inclination of the galactic disc, derived by Sakhibov & Smirnov (2004). Other parameters were taken from the LEDA data base¹ (Paturel et al. 2003). We adopt the Hubble constant $H_0 = 75 \text{ km s}^{-1} \text{ Mpc}^{-1}$ in the paper. With the assumed distance to NGC 628, we estimate a linear scale of $34.9 \text{ pc arcsec}^{-1}$.

Observations and reduction stages of *UBVRI* images for NGC 628 have already been published in Bruevich et al. (2007). The reduction of the photometric data was carried out using standard techniques, with the European Southern Observatory Munich Image Data Analysis System² (ESO-MIDAS).

2 IDENTIFICATION AND SIZE ESTIMATIONS OF STAR FORMATION REGIONS

In Bruevich et al. (2007), we have identified star formation regions in the galaxy with the list of H II regions of Belley & Roy (1992), based on their H α spectrophotometric data. The list of Belley & Roy (1992) is still the most complete survey of H II regions and their parameters in NGC 628. Note that our coordinate grid coincides with that of Kennicutt & Hodge (1980) and is systematically shifted with respect to that of Belley & Roy (1992). Altogether, we identified 127 of 132 SFRs studied in Belley & Roy (1992). Three regions (Nos. 1, 2, and 96 in Belley & Roy 1992) were outside the field of view of our images. Two SFRs (Nos. 23 and 76) are missing in the list of Belley & Roy (1992). Belley & Roy (1992) did not distinguish between isolated SFRs, with typical sizes about 60-70 pc, and compound multi-component regions, with typical sizes about 200 pc. We obtained images of the galaxy with better seeing than Belley & Roy (1992). As a result, we were able to resolve the compound SFRs into components.

Firstly, we identified such subcomponents by eye. We selected the components, the maximal (central) brightness in which was at least 3 times higher than the brightness of surrounding background. Next, we fitted profiles of SFRs using Gaussians. The components separation condition was that the full width at half-maximum (FWHM) of the region is less than the distance between centres of Gaussians. Numbers of these complexes in the first column of Table A1 contain additional letters: 'a', 'b', 'c', and 'd'. Compound regions which do not satisfy this condition were classified as objects with observed, but unresolved, internal structure. In total, we identified 186 objects (Fig. 1).

In this paper we use the numbering order adopted in Bruevich et al. (2007). It coincides with the numbering order of Belley & Roy (1992) with the exception of the missed SFRs.

We found that 146 regions from Table A1 have a star-like profile (see the last column in this table). Other 40 objects have a non-star-like (extended (diffuse) or multi-component) profile, i.e. these objects have an observed, but unresolved, internal structure.

We took the geometric mean of major and minor axes of a star formation region for the SFR's characteristic diameter d : $d = \sqrt{d_{\max} \times d_{\min}}$. We measured d_{\max} and d_{\min} from the radial V profiles as the FWHM for regions having a star-like profile, or as the distance between points of maximum flux gradient for regions having non-star-like profiles. We adopted seeing for the uncertainty in the size measurements, which definitely exceeds all other errors. Obtained parameters of SFRs are presented in Table A1.

3 HIERARCHICAL STRUCTURES OF STAR FORMATION REGIONS

The simplest way to study hierarchical clustering is to identify structures of different hierarchical levels based on lower level surface brightness thresholds above the background level. The similar method was used by Gouliermis et al. (2010), who used the stellar density levels to study hierarchical stellar structures in the dwarf irregular galaxy NGC 6822. They identified hierarchical structures using density thresholds $1\sigma - 5\sigma$ above the average background density level with step of 1σ .

However, this direct way is not applicable for identification of hierarchical structures in NGC 628. The background level varies

¹ <http://leda.univ-lyon1.fr/>

² <http://www.eso.org/sci/software/esomidas/>

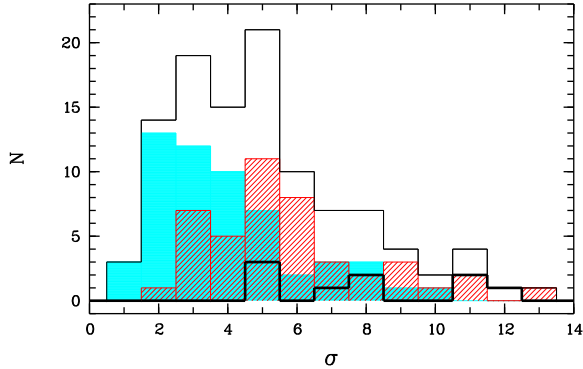


Figure 3. Distribution histogram of SFRs of Levels 2-5 by the level of maximum brightness decrease. Brightness is given in units of σ . Grey histogram is the distribution of SFRs of the lowest hierarchical level. Shaded histogram is the distribution of SFRs of the first hierarchical level from the lowest one. Thick black histogram is the distribution of SFRs of the second hierarchical level from the lowest one. See the text for details.

significantly in the galactic plane. The surface brightness of the background differs by several times inside spiral arms and in interarm regions.

Therefore we modified the technique of Gouliermis et al. (2010). Identification and size estimation of 186 SFRs at the highest hierarchical level (Level 1) were done using their half-maximum brightness levels, independent of background levels (see Section 2). Additionally, we fitted the profiles of SFRs along their minor and major axes using Gaussians. To identify structures of Level 2 and lower, we measured the background surface brightness in the V passband in the vicinity of every group of SFRs of Level 1.

The selection of a threshold in units of σ above the average brightness level of background for SFRs of Level 2 was carried out based on two basic conditions: (i) it must be lower than the level of brightness of the appropriate SFR of Level 1 and (ii) it must deviate more than 4 pixels (seeing of the V image) from the fitting Gaussian of the profile of the SFR at Level 1. The same conditions were applied to select the brightness level of every next lower level of the hierarchy. The exception was made for several resolved close binary SFRs, such as 40a-40b, where the second condition is not applied. To identify SFRs of lower hierarchical levels, we used lower levels of brightness.

To select surface brightness thresholds, we firstly analysed a typical light distribution in selected SFRs and their vicinities. Example of such region, SFRs Nos. 33-35, is given in Fig. 2.

Fig. 2 (central panel) shows that the surface brightness falls irregularly with distance from the knots of star formation: ‘plateau-like’ areas with constant surface brightness alternate with areas of a sharp drop in brightness. At such sites, a fall in brightness usually exceeds 1σ value. At higher hierarchical levels, where the surface brightness is higher, absolute drop in brightness is larger than at lower levels of the hierarchy. As a result, diameters of SFRs increase slowly with a decrease of brightness level within the same hierarchical level. Significant growth of the diameters is observed only at merger of two separate SFRs into one common SFR at the lower hierarchical level (Fig. 2).

We consider brightness in units of σ . So the brightness level, where the maximum brightness decrease is observed, is also measured in units of σ . Maximum brightness decrease corresponds to the minimum of first derivative of the brightness profile function (Fig. 2, central panel) in units of σ . After measuring the bright-

ness level in units of σ by the maximum brightness decrease, we determine size of SFR with the isophots as described in Section 2.

We analysed all hierarchical structures in vicinities of SFRs of Level 1 and determined which level of brightness corresponds to the level of maximum brightness decrease in them (Fig. 3).

Distribution of SFRs of Levels 2-5 by the level of maximum brightness decrease shows two maxima at 3σ and 5σ (Fig. 3). Distribution of SFRs of the lowest hierarchical level has a maximum at $2\sigma - 3\sigma$, distribution of SFRs of the first hierarchical level from the lowest one shows maxima at 3σ and $5\sigma - 6\sigma$. SFRs of the second hierarchical level from the lowest one have characteristic levels of maximum brightness decrease of 5σ , 8σ , and 11σ (Fig. 3).

Analysis of the distribution of SFRs by the level of maximum brightness decrease, in units of σ , has shown that neither arithmetic nor geometric sequences of the brightness levels are suitable to describe the hierarchical structures of SFRs. When using a geometric sequence, we may miss some of the hierarchical levels. When using an arithmetic sequence, we lose some of the brightness levels because they do not satisfy the condition (ii) (Fig. 2). In this case, low hierarchical levels will correspond to arbitrary levels of brightness.

Analysis of the distribution showed that the best sequence of brightness levels is the Fibonacci sequence, 1σ , 2σ , 3σ , 5σ , 8σ , as an intermediate sequence between arithmetic and geometric sequences.

Diameters of SFRs of the lower hierarchical levels which have the maximum brightness decrease at the level of 4σ or $6\sigma - 7\sigma$ are measured at the next lower surface brightness level of 3σ or 5σ , respectively. Typically, the difference between diameters measured at the levels of 3σ and 4σ , or 5σ and $6\sigma - 7\sigma$ does not exceed 35-40 pc, a value of the seeing of the image (Fig. 2).

Thus, we used surface brightness thresholds of 8σ , 5σ , 3σ and 2σ above the average brightness level of background in the vicinity of SFR. The threshold of 1σ was not used due to large fluctuations of background around many identified groups of SFRs.

For each individual region, not every next lower brightness level satisfies the conditions adopted. Such brightness levels were missed. Furthermore, a full set of brightness levels from 8σ to 2σ above the background was used only for SFRs Nos. 79a and 79b and hierarchical structures of a lower order related with them (Table A2). The lowest level of every hierarchical structure usually corresponds to the brightness level of 2σ or 3σ above the background (Fig. 3). As a result, the same hierarchical level may correspond to different levels of brightness.

Diameters of SFRs at Levels 2 and lower were measured in the same manner as for SFRs of Level 1: $d = \sqrt{d_{\max} \times d_{\min}}$, where d_{\min} and d_{\max} are diameters along the major and minor axes of SFR.

SFRs obtained on different hierarchical levels, and their sizes are presented in Table A2. Some SFRs of low hierarchical levels consist of one or several star-like cores (SFRs of Level 1) and an extended halo. Such SFRs are indicated by letter ‘h’ in Table A2. A map of location of these objects in the galactic plane is shown in Fig. 4.

To illustrate the hierarchical structures we used so-called dendrograms. Dendrograms were introduced as ‘structure trees’ for analysis of molecular cloud structures by Houllahan & Scalo (1992), refined by Rosolowsky et al. (2008), and used in Gouliermis et al. (2010) to study hierarchical stellar structures in the nearby dwarf galaxy NGC 6822. A dendrogram is constructed by cutting an image at different brightnesses and identifying connected areas, while keeping track of the connection to surface brighter smaller structures (on a higher level) and surface fainter

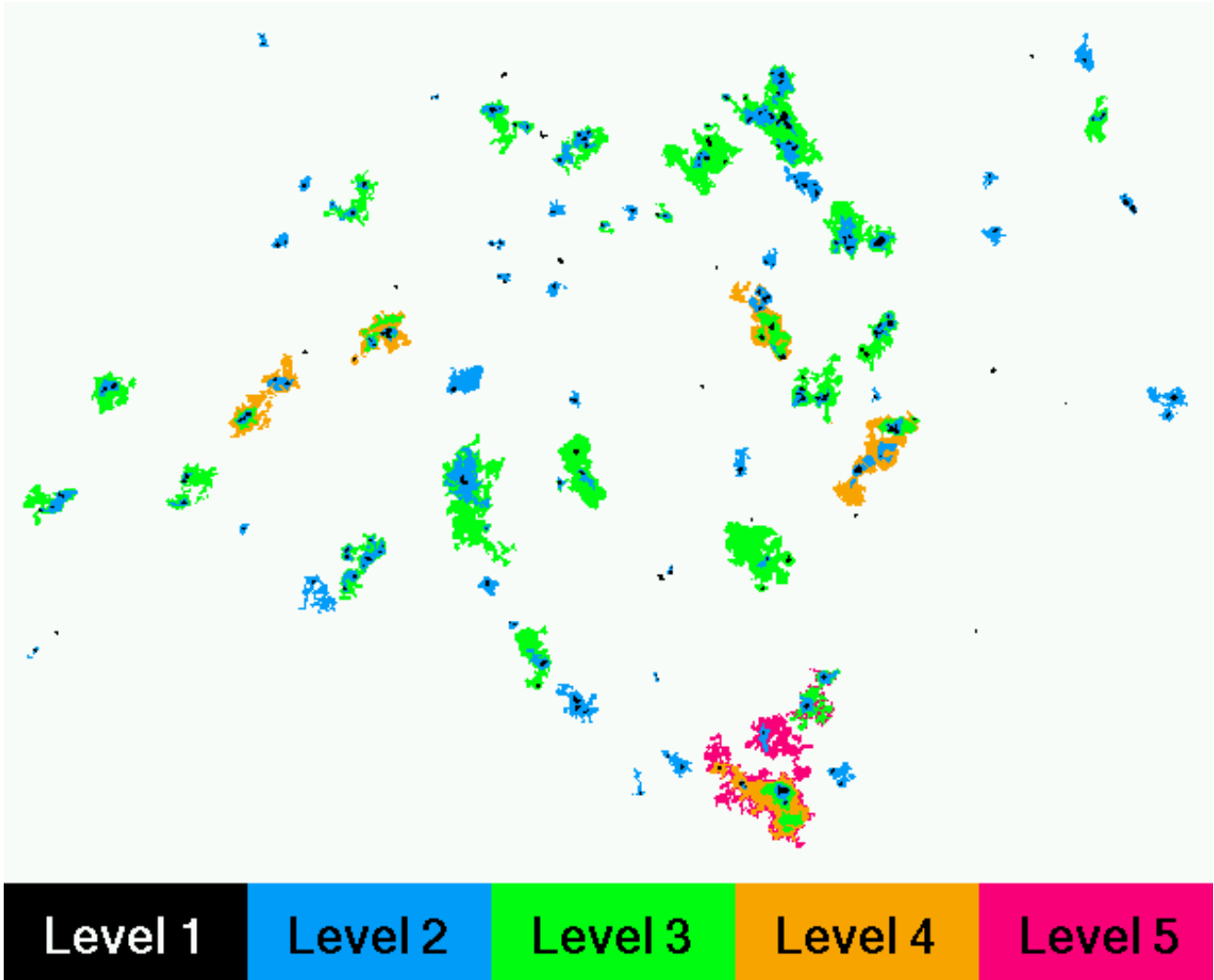


Figure 4. Map of star formation regions of different levels of the hierarchy. Regions of higher levels of the hierarchy are shaded darker than lower ones. The image size is 8.26×6.00 arcmin. North is upward and east is to the left.

larger structures (on the next lower level, which combines structures of the previous level).

The dendrogram for the SFRs from Tables A1 and A2 is presented in Fig. 5. Unlike Gouliermis et al. (2010), we constructed the dendrogram using the ordinate axis in units of diameter. It better illustrates length scales of hierarchical structures. The combination of this dendrogram with the map of Fig. 4 illustrates graphically the hierarchical spatial distribution of SFRs in NGC 628.

The dendrogram demonstrates that most SFRs are combined into larger structures over, at least, 1-2 levels. We found only 12 separate associations without visible internal structure, which are out of hierarchical structures (Fig. 5). Most of them are located in interarm regions (Fig. 1). The largest ($d > 1$ kpc) and the most populous (8-17 SFRs of Level 1) structures are located in the ends of spiral arms. First of them (Nos. 75-80) is located near the corotation radius, which was obtained in Sakhibov & Smirnov (2004) based on a Fourier analysis of the spatial distribution of radial velocities of the gas in the disc of NGC 628. Largest and brightest in UV star complex of the galaxy was found here in Gusev, Egorov & Sakhibov (2014). Second structure (Nos. 120-

127) is located in the northern-western part of NGC 628, in the disturbed part of the spiral arm (Fig. 1).

As seen from the dendrogram, the numbering order does not reflect correctly the hierarchical structures. The numbering is violated for SFRs Nos. 4-7 at Level 2, Nos. 85-89 at Level 4, and Nos. 97-109 at Level 4 (Table A2).

4 SIZE DISTRIBUTIONS OF STAR FORMATION REGIONS

In Fig. 6, we present size distribution histograms for three sets of SFRs under study. The first set includes 297 regions of all hierarchical levels, the second set is a sample of 146 associations with a star-like profile, and the third set includes 111 regions of Level 2 and lower from Table A2. The second set unites the SFRs without an observed internal structure; their subcomponents (if exist) have sizes $\leq 35 - 40$ pc. The third set includes only SFRs with obvious internal structure; their subcomponents were detected and measured.

As seen from the figure, associations with a star-like profile

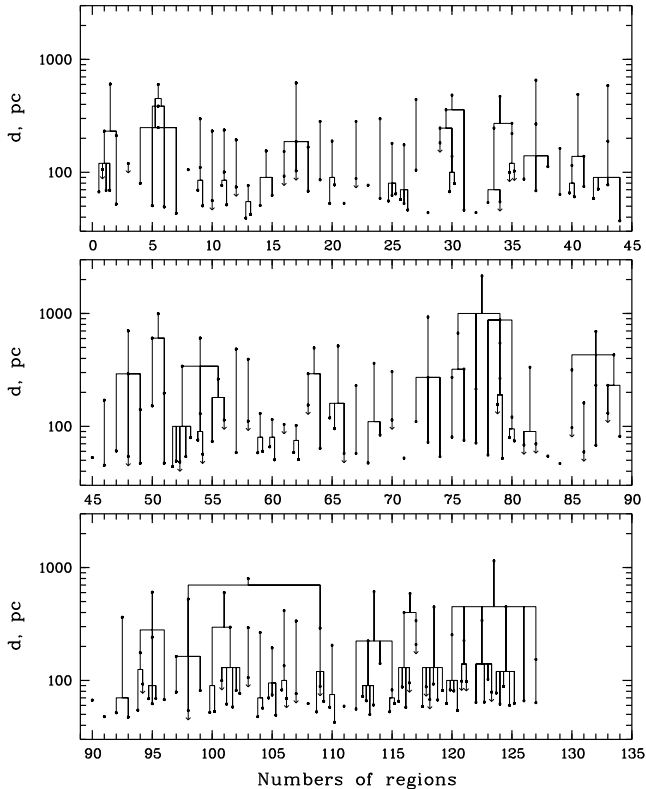


Figure 5. Dendrogram of star formation regions structures. The black dots indicate star formation regions from Tables A1, A2. Regions which are united into a hierarchical structure are connected by solid line. The numbering order might not strictly follow the order of hierarchical structures (see the text for details). The arrows down indicate star formation regions with an observed internal structure (star formation regions with a non-star-like profile).

have a narrow range of sizes, from 40 to 100 pc, with a few exceptions. The mean diameter of these SFRs is equal to 66 ± 18 pc. This is a typical size of OB associations. SFRs with extended profile have, on average, slightly larger sizes, ~ 100 pc. As a result, the size distribution of SFRs of Level 1 with both star-like and extended profiles is displaced a little toward the larger sizes (see Fig. 6 and Table 2).

SFRs of lower levels clearly show a bimodal size distribution. Two maxima at ≈ 250 and ≈ 600 pc are observed (Fig. 6). The first smoothed peak corresponds to a characteristic size of stellar aggregates by classification of Efremov et al. (1987), and the second peak is located on diameters, which are typical for star complexes.

We also fitted size distributions of studied sets of SFRs using Gaussians. To fit the size distribution for the set of 111 complex SFRs, we used a combination of two Gaussians. It was found that all sets of SFRs have size distributions close to the Gaussian distribution. Diameters obtained from the best-fit Gaussians are almost the same as the mean diameters for all sets of SFRs (Table 2).

Following Elmegreen et al. (2006), we constrained the cumulative size distribution function in the form $N(d > D) \propto D^\gamma$, where N is the integrated number of objects that have a diameter d greater than some diameter D (Fig. 7).

Detailed exploration of the size distribution of objects in NGC 628 was made in Elmegreen et al. (2006) in the range of

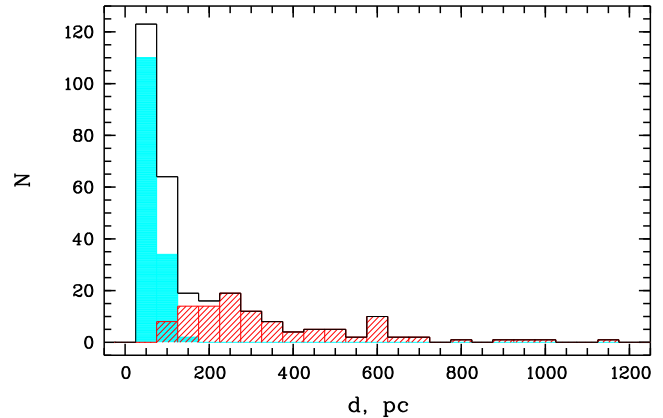


Figure 6. Number distribution histograms of all star formation regions from Tables A1 and A2, SFRs of Level 1 with a star-like profile (grey histogram), and SFRs of Levels 2 and lower (shaded histogram).

scales from 2 to 110 pc³ based on *HST* images. For regions in the central part of the galaxy brighter than the 3σ noise limits in *B* and *V* images, Elmegreen et al. (2006) found that the cumulative size distribution obeys a power law, with a slope $\gamma \approx -1.5$ in the range from 2 to 55 pc. The similar slope of the cumulative size distribution function was found for OB associations from the list of Ivanov et al. (1992) in the range from 30 to 110 pc. The size distribution of larger objects, H II regions studied by Hodge (1976), satisfies a power law with a slope $\gamma \approx -3.5$ in the range from 100 to 300 pc. The size distribution of large SFRs (in the range from 300 to 600 pc) in spiral arms of NGC 628 obtained in Gusev et al. (2014) shows a slope $\gamma \approx -4.5$. The size distribution of complexes from Ivanov et al. (1992) gives $\gamma = -4.1$ in the range from 500 to 1000 pc (Fig. 7).

Summarizing the results of the size distribution obtained previously, we can conclude that the size distributions of SFRs with a diameter of ≤ 100 pc satisfy a power law with $\gamma \approx -1.5$. The distribution of larger SFRs obeys a power law with γ between ≈ -5 and ≈ -3.5 .

In Fig. 7 (right panel) we present size distribution functions constructed for three sets of SFRs. The first set includes 297 regions of all hierarchical levels, the second set is a sample of 186 SFRs of Level 1, and the third set includes 146 regions of Level 1 with star-like profile.

Size distribution of 146 SFRs with a star-like profile, beginning with $d \approx 50$ pc, obeys a power law with a slope $\gamma \approx -5$. Size distribution of all 186 SFRs of Level 1 satisfies a power law with a slope $-4 \leq \gamma \leq -3.5$ in the range from 50 to 170 pc. It repeats the distribution of H II regions of Hodge (1976) with a displacement $\log D \approx 0.2$ (Fig. 7). In general, the size distribution of SFRs of Level 1 has slopes between -5 and -3.5 , such as size distributions of previously studied SFRs of a single level of hierarchy (Fig. 7).

Note, that the end of the size distribution curve for regions of Elmegreen et al. (2006) coincides with the beginning of the size distribution curve for our 186 SFRs of Level 1 (Fig. 7). Given that the area studied in Elmegreen et al. (2006) occupies $\sim 70\%$ of the area of NGC 628, which is studied in this paper, we can conclude that (i) the number of H II regions identified in Belley & Roy (1992) is smaller than the numbers of re-

³ For an adopted distance of 7.2 Mpc.

Table 2. Diameters of star formation regions.

SFRs	d^a (pc)	d^b (pc)
Associations ^c	66 ± 18	64
Associations ^d	72 ± 26	66
Aggregates	240 ± 90	234
Complexes	583 ± 84	601

^a Mean diameter. ^b Diameter obtained from best fitting Gaussian.

^c Associations with a star-like profile (146 objects).

^d All associations from Table A1 (186 objects).

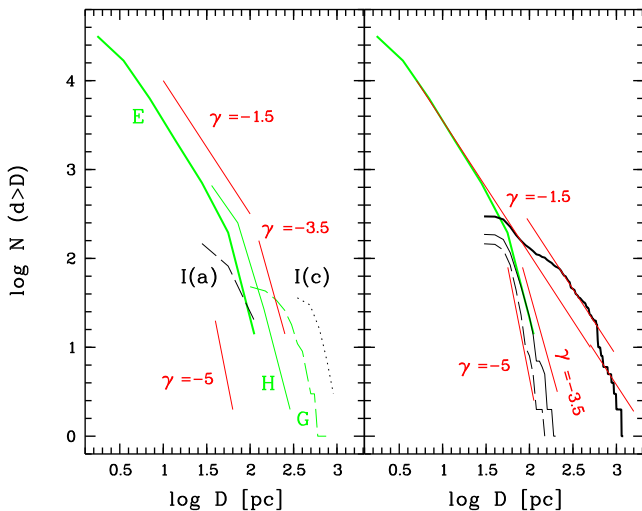


Figure 7. Left panel: cumulative size distribution functions for regions of Elmegreen et al. (2006) (E; grey thick solid curve), H II regions of Hodge (1976) (H; grey thin solid curve), associations (I(a); black dashed curve) and complexes (I(c); black dotted curve) of Ivanov et al. (1992), large star formation regions in the spiral arms of the galaxy (G; grey thin dashed curve) from Gusev et al. (2014). Right panel: cumulative size distribution functions for regions of Elmegreen et al. (2006) (grey thick solid curve), 146 SFRs with a star-like profile from Table A1 (black dashed curve), 186 SFRs from Table A1 (black solid curve), and 297 SFRs from Tables A1 and A2 (black thick curve). Dark thin solid straight lines in both panels represent slopes $\gamma = -1.5$, -3.5 and -5 of the size distribution function. See the text for details.

regions found by Elmegreen et al. (2006) using SExtractor, and, that is more important, (ii) our measurements of sizes of SFRs using photometric profiles are in a good agreement with measurements of Elmegreen et al. (2006).

More interesting behaviour is observed for the curve of size distribution of SFRs of all hierarchical levels. It continues the size distribution curve for regions of Elmegreen et al. (2006) at $d = 30 - 40$ pc and has the same slope ≈ -1.5 in the range from 45 to 85 pc – diameters of OB associations. Flatter slope, $\gamma > -1$, is observed in the range from ≈ 90 to ≈ 180 pc for regions of Level 1 with an extended profile and for the smallest regions of Level 2. Size distribution of SFRs, which are classified as stellar aggregates and complexes, obeys a power law with $\gamma = -1.5$ very well (see the distribution curve in the range from 190 to 600 pc in Fig. 7). Largest hierarchical structures with $d = 0.65 - 0.9$ kpc are also distributed by sizes by a power law with $\gamma \sim -1.5$ (Fig. 7).

Thus, the size distribution of SFRs of all hierarchical levels continues the size distribution function for regions of Elmegreen et al. (2006) towards the larger sizes with the same slope ≈ -1.5 .

5 DISCUSSION

The modern theory of star formation explains an existence of OB associations and star complexes, which are associated by unity of an origin with hydrogen superclouds and giant molecular clouds, respectively (Efremov & Elmegreen 1998; Elmegreen & Efremov 2006). Structures of H_2 on the intermediate scale length are unknown. However, such intermediate young stellar structures are observed in galaxies. These are stellar aggregates with diameters $\sim 200 - 300$ pc.

Our Fig. 6 shows a bimodal size distribution of SFRs of Level 2 and lower. Bimodal size distributions with a secondary peak at $d = 150 - 300$ pc were found for ‘associations’ in SMC (Battinelli 1991), M31 (Magnier et al. 1993), NGC 2090, NGC 2541, NGC 3351, NGC 3621 and NGC 4548 (Bresolin et al. 1998), NGC 1058 and UGC 12732 (Battinelli et al. 2000), NGC 300 (Pietrzyński et al. 2001), NGC 3507 and NGC 4394 (Vicari et al. 2002), NGC 7793 (Pietrzyński et al. 2005). Pietrzyński et al. (2005) named such ‘associations’ ‘superassociations’.

Thus, the existence of stellar structures, ‘aggregates’ or ‘superassociations’, with a characteristic size 200–300 pc is confirmed by numerous observations in different galaxies. However, the question of origin of stellar aggregates is still open.

As we noted above, the size distribution of SFRs of all hierarchical levels continues the size distribution of regions of Elmegreen et al. (2006) with the same slope ≈ -1.5 for sizes from 45 pc to ~ 0.9 kpc. However, the function of size distribution deviates from a power law with the slope -1.5 at $d = 90 - 180$ pc and 600 – 650 pc (Fig. 7).

We believe that the flatter slope in the range of 90 to 180 pc is a result of significant number of SFRs with a diameter of $\sim 100 - 150$ pc with an unresolved internal structure. Taking into account such undetected objects will shift the distribution curve upward along the ordinate axis at sizes smaller than or equal to diameters of these SFRs.

Opposite situation is observed at $d = 600 - 650$ pc. Largest structures with $d > 600$ pc have a low boundary surface brightness. They are difficult for identification in spiral arms of grand design galaxy NGC 628 because of the significant variations of background level (see Section 4). Underestimation a number of SFRs at lowest hierarchical levels leads to a drastic drop in the size distribution curve.

In spite of small statistics, largest SFRs with $d \approx 0.65 - 0.9$ kpc are also distributed by size by a power law with $\gamma \sim -1.5$. It can be an additional argument in favor of the assumption of Efremov et al. (1987), Elmegreen & Efremov (2006) and Zhang et al. (2001), who adopted that the hierarchical structures extend to the scale of 1 kpc.

Taking into account the hierarchy of SFRs is crucial for construction of the cumulative size distribution function. Neglecting the internal structure of SFRs of higher hierarchical levels and underestimation of the number of SFRs of lower hierarchical levels leads to a decrease or an increase of the slope of the size distribution function, respectively. To illustrate this, we compare size distributions of regions of Elmegreen et al. (2006), our SFRs of all

hierarchical levels, and our SFRs of Level 1 with any profiles in the range of scale from 50 to 110 pc in Fig. 7.

On the scale of 200–600 pc, the characteristic sizes of stellar aggregates and complexes, the size distribution function has a constant slope. We believe that the sample of objects at different levels of hierarchy within this range of scale is complete.

The slope γ of the cumulative size distribution function for SFRs is of fundamental importance. It is associated with the fractal dimension of objects in the galaxy at different scales. Elmegreen et al. (2006) introduced the fractal of dimension \mathcal{D} , where $\mathcal{D} = -\gamma$. Following Elmegreen et al. (2006), we believe that the size distribution of stellar groups suggests a fractal distribution of stellar positions projected on the disc of the galaxy, with a constant fractal dimension of $\mathcal{D} \approx 1.5$ in the wide range of length scales from 2 pc to 1 kpc. It is comparable to the fractal dimension of projected local interstellar clouds, $\mathcal{D} \approx 1.3$ (Falgarone, Phillips & Walker 1991), and to the fractal dimension of H I ($\mathcal{D} = 1.2 - 1.5$) in the M81 group of galaxies (Westpfahl et al. 1999).

6 CONCLUSIONS

We studied hierarchical structures and the size distribution of star formation regions in the spiral galaxy NGC 628 over a range of scale from 50 to 1000 pc based on size estimations of 297 SFRs. Most star formation regions are combined into larger structures over several levels. We found three characteristic sizes of young star groups: OB associations with mean diameter $d = 66 \pm 18$ pc, stellar aggregates ($d = 240 \pm 90$ pc) and star complexes (583 ± 84 pc).

The cumulative size distribution function of star formation regions satisfies a power law with a slope of -1.5 at scales from 45 to 85 pc, from 190 to 600 pc, and from 650 pc to 900 pc, which are appropriate to the sizes of associations, aggregates and complexes. Together with the result of Elmegreen et al. (2006), who found the slope $-1.8 \leq \gamma \leq -1.5$ for regions at scales from 2 to 100 pc, our result shows that the size distribution of young stellar structures in the galaxy obeys a power law with a constant slope of ≈ -1.5 at all studied scales from ≈ 2 pc to ≈ 1 kpc.

Ignoring the hierarchical structures, i.e. using SFRs of only one of hierarchical levels to examine the size distribution, gives slopes $-5 \leq \gamma \leq -3$.

ACKNOWLEDGEMENTS

The author is grateful to the referee for his/her constructive comments. The author is grateful to Yu. N. Efremov (Sternberg Astronomical Institute) for useful discussions. The author thanks E. V. Shimanovskaya (Sternberg Astronomical Institute) for help with editing this paper. The author acknowledges the usage of the HyperLeda data base (<http://leda.univ-lyon1.fr>). This study was supported in part by the Russian Foundation for Basic Research (project nos. 12-02-00827 and 14-02-01274).

REFERENCES

Ballesteros-Paredes J., Klessen R. S., MacLow M.-M., Vazquez-Semadeni E., 2007, in Reipurth B., Jewitt D., Keil K., eds, *Protostars and Planets V*. Univ. of Arizona Press, Tucson, p. 63

Bastian N., Gieles M., Efremov Yu. N., Lamers H. J. G. L. M., 2005, *A&A*, 443, 79
 Battinelli P., 1991, *A&A*, 244, 69
 Battinelli P., Efremov Y., Magnier E. A., 1996, *A&A*, 314, 51
 Battinelli P., Capuzzo-Dolcetta R., Hodge P. W., Vicari A., Wyder T. K., 2000, *A&A*, 357, 437
 Belley J., Roy J.-R., 1992, *ApJS*, 78, 61
 Bianchi L., Efremova B., Hodge P., Kang Y., 2012, *AJ*, 144, 142
 Borissova J., Kurtev R., Georgiev L., Rosado M., 2004, *A&A*, 413, 889
 Brandeker A., Jayawardhana R., Najita J., 2003, *AJ*, 126, 2009
 Bresolin F., Kennicutt R. C., Jr., Stetson P. B., 1996, *AJ*, 112, 1009
 Bresolin F. et al., 1998, *AJ*, 116, 119
 Bruevich V. V., Gusev A. S., Guslyakova S. A., 2011, *Astron. Rep.*, 55, 310
 Bruevich V. V., Gusev A. S., Ezhkova O. V., Sakhibov F. Kh., Smirnov M. A., 2007, *Astron. Rep.*, 51, 222
 Dahm S. E., Simon T., 2005, *AJ*, 129, 829
 de la Fuente Marcos R., de la Fuente Marcos C., 2009, *ApJ*, 700, 436
 Efremov Yu. N., 1989, *Sites of Star Formation in Galaxies: Star Complexes and Spiral Arms*. Fizmatlit, Moscow, p. 246 (in Russian)
 Efremov Yu. N., 1995, *AJ*, 110, 2757
 Efremov Yu. N., Elmegreen B. G., 1998, *MNRAS*, 299, 588
 Efremov Yu. N., Ivanov G. R., Nikolov N. S., 1987, *Ap&SS*, 135, 119
 Elmegreen B. G., 1994, *ApJ*, 433, 39
 Elmegreen B. G., 2002, *ApJ*, 564, 773
 Elmegreen B. G., 2006, in Del Toro Iniesta J. C. et al., eds, *The Many Scales in the Universe: JENAM 2004 Astrophysics Reviews*. Springer, Dordrecht, p. 99
 Elmegreen B. G., 2009, in Andersen J., Bland-Hawthorn J., Nordström B., eds, *Proc. IAU Symp. 254, The Galaxy Disk in Cosmological Context*. Kluwer, Dordrecht, p. 289
 Elmegreen B. G., 2011, in Charbonnel C., Montmerle T., eds, *Ecole Evry Schatzman 2010: Star Formation in the Local Universe*. EAS Publications Series, 51. Cambridge Univ. Press, Cambridge, p. 31
 Elmegreen B. G., Efremov Yu. N., 1996, *ApJ*, 466, 802
 Elmegreen B. G., Elmegreen D. M., 2001, *AJ*, 121, 1507
 Elmegreen B. G., Elmegreen D. M., Leitner S. N., 2003a, *ApJ*, 590, 271
 Elmegreen B. G., Efremov Y., Pudritz R. E., Zinnecker H., 2000, in Mannings V., Boss A. P., Russell S. S., eds, *Protostars and Planets IV*. Univ. of Arizona Press, Tucson, p. 179
 Elmegreen B. G., Leitner S. N., Elmegreen D. M., Cuillandre J.-C., 2003b, *ApJ*, 593, 333
 Elmegreen B. G., Elmegreen D. M., Chandar R., Whitmore B., Regan M., 2006, *ApJ*, 644, 879
 Falgarone E., Phillips T., Walker C. K., 1991, *ApJ*, 378, 186
 Feitzinger J. V., Braunsfurth E., 1984, *A&A*, 139, 104
 Gouliermis D. A., Schmeja S., Klessen R. S., de Blok W. J. G., Walter F., 2010, *ApJ*, 725, 1717
 Gusev A. S., 2002, *Astron. Astrophys. Trans.*, 21, 75
 Gusev A. S., Egorov O. V., Sakhibov F., 2014, *MNRAS*, 437, 1337
 Harris J., Zaritsky D., 1999, *AJ*, 117, 2831
 Heydari-Malayeri M., Charmandaris V., Deharveng L., Rosa M. R., Schaerer D., Zinnecker H., 2001, *A&A*, 372, 495
 Hodge P. W., 1976, *ApJ*, 205, 728
 Houlahan P., Scalo J., 1992, *ApJ*, 393, 172

- Ivanov G. R., 1991, Ap&SS, 178, 227
Ivanov G. R., Popravko G., Efremov Y. N., Tichonov N. A., Karachentsev I. D., 1992, A&AS, 96, 645
Kennicutt R. C., Hodge P. W., 1980, ApJ, 241, 573
Krumholz M. R., McKee C. F., 2005, ApJ, 630, 250
Kumar M. S. N., Kamath U. S., Davis C. J., 2004, MNRAS, 353, 1025
Larsen S. S., 1999, A&AS, 139, 393
Larson R. B., 1981, MNRAS, 194, 809
Magnier E. A. et al., 1993, A&A, 278, 36
Odekon M. C., 2008, ApJ, 681, 1248
Oey M. S., Watson A. M., Kern K., Walth G. L., 2005, AJ, 129, 393
Paturel G., Petit C., Prugniel Ph., Theureau G., Rousseau J., Brouty M., Dubois P., Cambresy L., 2003, A&A, 412, 45
Pietrzyński G., Gieren W., Fouqué P., Pont F., 2001, A&A, 371, 497
Pietrzyński G., Ulaczyk K., Gieren W., Bresolin F., Kudritzki R. P., 2005, A&A, 440, 783
Rosolowsky E. W., Pineda J. E., Kauffmann J., Goodman A. A., 2008, ApJ, 679, 1338
Sakhibov F. Kh., Smirnov M. A., 2004, Astron. Rep. 48, 995
Sánchez N., Añez N., Alfaro E. J., Crone Odekon M., 2010, ApJ, 720, 541
Sánchez-Monge Á. et al., 2013, MNRAS, 432, 3288
Sharina M. E., Karachentsev I. D., Tikhonov N. A., 1996, A&AS, 119, 499
van Dyk S. D., Li W., Filippenko A. V., 2006, PASP, 118, 351
Vicari A., Battinelli P., Capuzzo-Dolcetta R., Wyder T. K., Arrabito G., 2002, A&A, 384, 24
Westpfahl D. J., Coleman P. H., Alexander J., Tongue T., 1999, AJ, 117, 868
Wilson C. D., 1991, AJ, 101, 1663
Wilson C. D., 1992, ApJ, 386, L29
Zhang Q., Fall S. M., Whitmore B. C., 2001, ApJ, 561, 727

APPENDIX A: PARAMETERS AND HIERARCHICAL STRUCTURES OF STAR FORMATION REGIONS

Table A1. Identification, offsets, and diameters of star formation regions.

ID	ID (BR) ^a	N-S ^b (arcsec)	E-W ^b (arcsec)	<i>d</i> (pc)	Note	ID	ID (BR)	N-S (arcsec)	E-W (arcsec)	<i>d</i> (pc)	Note	ID	ID (BR)	N-S (arcsec)	E-W (arcsec)	<i>d</i> (pc)	Note
1a	3	+108.8	-40.3	65	st ^c	48	51	-29.1	-40.1	55		97	102	+17.8	+42.9	80	st
1b	3	+106.9	-38.5	105		49	52	-33.6	-48.9	45	st	98	103	+25.8	+33.8	55	
1c	3	+104.2	-37.4	70	st	50	53	-32.8	-88.3	150	st	99	104	+30.4	+38.3	80	st
1d	3	+110.4	-36.6	70	st	51	54	-52.3	-78.5	45	st	100a	105	+21.0	+75.1	50	st
2	4	+98.4	-48.6	50	st	52a	55	-57.1	-126.2	45	st	100b	105	+18.9	+77.0	55	st
3	5	+109.0	-54.5	120		52b	55	-62.2	-122.7	50	st	101a	106	+27.2	+81.0	100	
4	6	+112.2	-61.9	80	st	52c	55	-59.5	-121.7	50		101b	106	+28.2	+83.4	60	st
5	7	+119.7	-72.9	50	st	53a	56	-67.5	-129.4	55	st	102a	107	+30.6	+82.9	60	st
6	8	+119.2	-76.1	50	st	53b	56	-64.8	-127.0	80	st	102b	107	+31.7	+86.9	80	st
7	9	+112.8	-67.0	45	st	54a	57	-64.3	-135.8	75	st	102c	107	+34.9	+86.1	75	st
8	10	+132.8	-72.3	105	st	54b	57	-61.6	-136.3	55		103	108	+69.0	+129.8	105	
9a	11	+75.5	-4.9	70	st	55	58	-72.0	-132.6	75	st	104a	109	+89.6	+127.7	50	st
9b	11	+76.0	-8.6	50	st	56	59	-76.6	-136.9	115		104b	109	+92.0	+127.7	55	st
10	12	+78.1	-18.7	55		57	60	-74.4	-149.9	60	st	105a	110	+78.6	+186.1	70	st
11a	13	+71.7	-31.3	75	st	58	61	-74.4	-77.9	110		105b	110	+81.1	+183.4	75	st
11b	13	+72.0	-28.9	50	st	59a	62	-91.0	-68.9	60	st	105c	110	+83.2	+182.9	50	st
12	14	+77.1	-51.5	75		59b	62	-91.5	-67.0	60	st	106a	111	+115.2	+170.3	80	st
13a	15	+124.0	-101.1	40	st	60a	63	-70.7	-3.3	65	st	106b	111	+116.8	+174.3	70	
13b	15	+124.2	-99.3	40	st	60b	63	-68.6	-2.7	50	st	107	112	+139.4	+166.6	75	
14	16	+145.8	-170.2	50	st	61	64	-72.6	-7.3	105		108	113	+141.0	+145.0	60	st
15	17	+149.3	-170.7	65	st	62a	65	-112.3	-9.4	60	st	109a	114	+37.8	+33.5	55	st
16	18	+88.3	-128.9	90		62b	65	-114.2	-8.6	50	st	109b	114	+41.6	+36.2	90	
17	19	+77.3	-133.7	105		63	66	-107.8	-55.5	155		109c	114	+44.2	+33.0	65	st
18	20	+80.3	-141.9	70	st	64	67	-116.8	-57.7	65	st	110a	115	+56.8	+35.9	60	st
19	21	+88.8	-153.1	85	st	65a	68	-122.4	-42.2	120	st	110b	115	+56.0	+38.6	45	st
20a	22	+63.7	-164.6	55	st	65b	68	-125.4	-41.7	95	st	111	116	+54.4	+15.7	60	st
20b	22	+64.8	-161.4	75	st	66	69	-127.2	-37.4	60		112	117	+98.1	+18.6	55	st
21	24	+5.8	+9.5	55	st	67	70	-160.8	-15.8	60	st	113a	118	+96.5	+8.2	70	st
22	25	+0.2	-43.0	90		68	71	-145.6	-4.6	45	st	113b	118	+99.7	+8.2	65	st
23	26	+57.6	-48.6	75	st	69	72	-149.9	+1.3	85	st	113c	118	+101.3	+9.3	50	st
24	27	+46.1	-51.0	60	st	70	73	-28.8	+25.3	115		113d	118	+99.2	+11.4	60	st
25a	28	+50.9	-73.7	55	st	71	74	-48.3	+29.8	50	st	114	119	+105.0	+13.0	140	st
25b	28	+51.4	-69.9	60	st	72	75	-65.4	+45.0	110	st	115a	120	+112.2	+11.1	55	st
25c	28	+48.8	-71.3	65	st	73	77	-64.3	+36.5	70	st	115b	120	+112.2	+12.5	65	st
26a	29	+64.2	-76.6	55	st	74	78	-77.1	+34.3	55	st	116a	121	+64.8	+64.5	65	st
26b	29	+64.8	-73.4	55	st	75	79	-113.4	+59.7	80	st	116b	121	+66.1	+67.5	90	st
26c	29	+62.6	-73.7	45	st	76	80	-125.1	+52.5	75	st	116c	121	+66.9	+70.3	60	st
27	30	+4.5	-92.3	105	st	77	81	-136.6	+34.6	70	st	116d	121	+62.6	+70.3	95	
28	31	+46.4	-115.8	45	st	78	82	-150.4	+16.7	55	st	117	122	+65.3	+82.3	210	
29	32	+28.5	-118.5	180		79a	83	-160.0	+42.6	155		118a	123	+87.2	+49.5	60	st
30a	33	+25.0	-126.7	65	st	79b	83	-164.6	+43.9	50	st	118b	123	+88.5	+51.4	90	
30b	33	+22.9	-124.6	80	st	80a	84	-156.6	+25.8	80	st	118c	123	+88.2	+55.4	70	
31	34	+17.0	-133.1	45	st	80b	84	-158.4	+27.4	75	st	118d	123	+85.0	+56.7	95	st
32	35	+19.7	-153.1	45	st	81	85	-157.1	+66.9	70		119a	124	+90.1	+48.7	65	st
33	36	+6.9	-160.3	55	st	82	86	-151.8	+63.1	70		119b	124	+91.7	+46.9	80	st
34	37	+8.0	-165.7	55		83	87	-47.0	+73.0	55	st	120a	125	+104.2	+41.0	60	st
35a	38	-5.1	-176.1	100		84	88	-94.2	+121.8	45	st	120b	125	+105.3	+45.5	80	st
35b	38	-7.8	-179.3	100		85	89	-28.3	+73.5	95		120c	125	+104.2	+47.7	80	st
36	39	+3.7	-236.6	85	st	86	90	+1.6	+81.0	60		120d	125	+102.4	+47.4	55	st
37	40	+5.0	-235.0	70	st	87	91	-23.2	+82.9	70	st	121a	126	+113.3	+44.5	100	
38	41	+6.1	-231.5	110	st	88	92	-12.0	+87.7	130		121b	126	+116.8	+43.7	100	
39	42	-52.3	-178.5	65	st	89	93	-8.0	+97.5	80	st	122	127	+125.8	+40.7	65	st
40a	43	-30.7	-201.9	65	st	90	94	+12.5	+129.0	65	st	123a	128	+134.1	+38.6	65	st
40b	43	-33.1	-202.7	60	st	91	95	-1.4	+158.9	50	st	123b	128	+133.3	+42.1	100	st
41	44	-41.9	-201.9	75	st	92	97	-6.2	+200.7	50	st	123c	128	+130.4	+41.5	80	
42a	45	-38.4	-253.9	60	st	93	98	+1.3	+203.4	45	st	124a	129	+118.1	+33.3	75	st
42b	45	-39.0	-252.6	70	st	94a	99	+1.0	+57.0	55	st	124b	129	+117.8	+35.9	60	st
43	46	-43.8	-256.6	75	st	94b	99	+2.1	+61.0	95		124c	129	+116.0	+38.3	90	st
44	47	-45.1	-261.9	35	st	95a	100	+1.0	+51.1	70	st	125a	130	+114.6	+28.2	60	st
45	48	-95.0	-255.0	55	st	95b	100	+3.2	+49.3	60	st	125b	130	+115.7	+29.8	65	st
46	49	-102.2	-263.8	45	st	95c	100	+4.8	+50.1	70	st	126	131	+123.7	+27.4	65	st
47	50	-21.1	-41.9	60	st	96	101	+9.6	+51.1	70	st	127	132	+124.2	+19.7	65	st

^a ID number by Belley & Roy (1992). ^b Offsets from the galactic centre, positive to the north and west. ^c Star-like profile.

Table A2. Hierarchical structures of star formation regions.

Level 1	Level 2	Level 3	Level 4	Level 1	Level 2	Level 3	Level 4	Level 5	Level 1	Level 2	Level 3	Level 4
1a-d	1 (230) ^a	1,2 (605)		44					86	86h (160)		
2	2h ^b (210)			45					87	87h (230)		
3				46	46h (170)				88	88h (230)	88,89 (430)	
4	4,7 (250)	4-7 (600)		47		47-49 (700)			89			
5	5,6 (385)			48	48h (290)				90			
6				49	49h (140)				91			
7				50	50h (605)	50,51 (995)			92	92,93 (365)		
8				51	51h (195)				93			
9a,b	9 (110)	9h (300)		52a-c	52,53 (340)	52-56 (605)			94a,b	94 (175)	94-96 (605)	
10	10h (230)			53a,b					95a-c	95 (240)		
11a,b	11 (100)	11h (235)		54a,b	54 (130)				96			
12	12h (195)			55	55,56 (260)				97	97h (165)	97-99 (525)	97-99, 109 (800)
13a,b	13 (75)			56					98			
14	14,15 (155)			57	57h (485)				99			
15				58	58h (395)				100a,b		100-102 (600)	
16	16h (155)	16-18 (620)		59a,b	59 (130)				101a,b	101,102 (295)		
17	17h (185)			60a,b	60 (115)				102a-c			
18	18h (165)			61					103	103h (295)		
19	19h (280)			62a,b	62 (100)				104a,b	104 (265)		
20a,b	20 (200)			63	63h (290)	63,64 (495)			105a-c	105 (195)		
21				64					106a,b	106 (135)	106h (415)	
22	22h (280)			65a,b	65,66 (515)				107	107h (335)		
23				66					108			
24	24h (300)			67	67h (230)				109a-c	109 (290)		
25a-c	25 (180)			68	68,69 (360)				110a,b	110 (205)		
26a-c	26 (175)			69					111			
27	27h (440)			70	70h (305)				112		112-115 (610)	
28				71					113a-d	113 (225)		
29	29h (245)	29,30 (360)	29-31 (480)	72		72-74 (930)			114			
30a,b	30 (140)			73	73h (270)				115a,b	115 (80)		
31				74					116a-d	116 (400)	116,117 (590)	
32				75	75h (270)	75,76 (670)		75-80 (2150)	117	117h (340)		
33	33,34 (245)		33-35 (470)	76	76h (320)				118a-d	118,119 (445)		
34				77	77h (215)				119a,b			
35a,b	35 (220)	35h (270)		78			78-80 (875)		120a-d	120 (255)	120-127 (1145)	
36	36-38 (270)	36-38h (655)		79a,b	79 (265)	79h (545)			121a,b	121 (225)		
37				80a,b	80 (120)				122	122,123 (340)		
38				81	81,82 (335)				123a-c			
39	39h (165)			82					124a-c	124,125 (450)		
40a,b	40 (115)	40,41 (490)		83					125a,b			
41	41h (140)			84					126			
42a,b	42-44 (190)	42-44h (585)		85	85h (315)		85,87-89 (695)		127	127h (155)		
43												

^a Diameter. ^b Star formation region with halo.